A Vibration Energy Approach Used to Identify Temperature Trending in Railroad Tapered-Roller Bearings

Constantine M. Tarawneh

Department of Mechanical Engineering, College of Engineering and Computer Science, The University of Texas-Pan American, Edinburg, TX 78539-2999, USA

Rafael K. Maldonado, Arturo A. Fuentes and Javier A. Kypuros

The University of Texas-Pan American, Edinburg, TX, USA

(Received 16 July 2014; accepted 5 March 2014)

Bearing temperature trending is a phenomenon that has plagued the railroad industry for decades and has resulted in costly train stoppages and non-verified bearing removals. Initial experimental studies conducted at The University of Texas-Pan American to explore this troubling phenomenon identified potential sources for the abrupt changes in temperature exhibited by some railroad bearings. The authors hypothesize that vibration-induced roller-misalignment is the root cause for bearing temperature trending. Hence, subsequent research focused on providing validation for the proposed hypothesis through vibration monitoring techniques. To that end, dynamic testers were used to run railroad bearings at the various speeds and loads that they experience in the field. A "trigger" bearing with a known cup raceway defect was used as a vibration source to induce roller misalignment on neighbouring defect-free bearings. Results show that the vibration energy of a bearing would decrease prior to an increase in temperature. In theory, misaligned rollers would vibrate less, leading to a decrease in the overall vibration energy, while also generating sufficient friction to account for the observed temperature increase. Typically, rollers realign themselves through geometrical thermal expansions or changes in the operating conditions, thus, returning to normal temperature and vibration levels. This paper outlines the research findings.

NOMENCLATURE

B_{d}	mean diameter of a roller
D_{cone}	cone tapered large end diameter
D_{l}	roller large end diameter
D_{roller}	roller mean diameter
D_{s}	roller small end diameter
L	cone raceway tapered length
N_{b}	number of rollers
P_{d}	pitch diameter (span between the centres of two opposite rolling elements)
R_{cone}	radius of the cone
R_{cup}	radius of the cup
α_{roller}	roller apex angle
θ	contact angle between the cone raceway and tapered roller
ϕ_{cone}	cone raceway tapered angle
ω_{cage}	fundamental frequency of the cage
ω_{cone}	fundamental frequency of the cone
ω_{in}	fundamental frequency of a roller passing over a defect on the cone raceway
ω_{o}	rotational frequency of the axle
ω_{out}	fundamental frequency of a roller passing over a defect on the cup raceway
ω_{roller}	fundamental frequency of the roller
$\omega_{\mathrm{rolldef}}$	fundamental frequency of a roller defect as it contacts the cup and cone raceway
BPFI	ball pass frequency inner race or cone
BPFO	ball pass frequency outer race or cup
BSF	ball spin or roller/cage frequency
FTF	fundamental train/cage frequency
HBD	hot-box detector
PS	power spectrum
PSD	power spectral density

1. INTRODUCTION

One of the main concerns troubling railroad bearing manufacturers is the unexplained abrupt increase in the operating temperature of a healthy (defect-free) tapered-roller bearing—a phenomenon referred to in field service as bearing temperature trending. Currently, trended bearings are removed from service since they exhibit similar behaviour to a burn-off bearing at the end of its life. This troubling phenomenon has resulted in many costly delays associated with train stoppages, as well as false bearing removals by wayside temperature monitoring devices such as the Hot Box Detector (HBD). According to data collected by Amsted Rail from 2001 to 2007, an average of nearly 40% of bearing removals are non-verified. A non-verified bearing is one that, upon disassembly and inspection, is found not to exhibit any of the commonly documented causes of bearing failure such as: spalling, water contamination, loose bearings, broken components, lubrication, damaged seals, etc.

HBDs measure the infrared radiation emissions present in a railroad bearing and have been in place since the 1950's. The HBD is set to trigger an alert when a bearing is running 94.4°C (170°F) above ambient conditions. However, a more recent approach adopted by some railroads utilizes the HBD data to compare each bearing's temperature to the average tempera-

ture of all bearings along the same side of the train. If a bearing is running significantly hotter than the average temperature by some predetermined threshold, it is removed from field service and labelled as "trended."[1]

In addition to the HBDs, acoustic measuring devices known as the Trackside Acoustic Detection System (TADS®) have been used in the field to identify defective bearings. The success rate of capturing a defective bearing is heavily based on the severity of the defect. Bearings with large defects known as "growlers" have a much higher rate of being recognized as opposed to bearings with smaller defects.[2] Although nearly five thousand HBDs are currently in service, only fifteen TADS® have been implemented in North America,[3] which means a train can run thousands of miles before encountering an acoustic bearing detector. Furthermore, the majority of trended bearings are found to be defect-free, which means that TADS® will not detect them.

From the above discussion, it is evident that the existing wayside monitoring equipment utilized in field service does not constitute a true continuous bearing health monitoring system, but rather a sporadic check on the bearing condition. Thus, neither temperature nor acoustic measuring devices, currently in use, can accurately characterize the internal condition of a temperature-trended bearing. To this end, the railroad research group at the University of Texas-Pan American (UTPA) conducted a series of experimental and theoretical studies focused at understanding the bearing temperature trending phenomenon and its root causes, with the main objective of finding ways to distinguish healthy (defect-free) bearings undergoing temperature trending from defective bearings nearing catastrophic failure. The latter will aid the railroad industry in minimizing unnecessary train stoppages and false bearing removals.

2. BACKGROUND

Thermal investigations of roller bearings have been carried out for a few decades now.[4–8] These efforts range from purely theoretical works to studies containing a combination of theory and application to purely experimental projects. The theoretical studies examined two abnormal operating conditions: partially or fully jammed roller bearings and a stuck brake. A partially jammed roller bearing is one that rotates with velocities greater than zero but less than the epicyclical speed, while a fully jammed roller bearing is one that has no velocity with respect to the cage. The investigation into the jammed rollers and a stuck brake condition revealed that the maximum temperature within the bearing assembly can reach 268°C (514°F) and 126°C (259°F), respectively, compared to the normal operating condition temperature of 81°C (178°F).[5,6] In a similar study, a dynamic model of the torque and heat generation rate in tapered-roller bearings under excessive sliding conditions was developed using a lumped-parameter approach in the program SHABERTH.[7] This investigation focused on jammed roller bearings, and the model was run with an assumed ambient temperature of 25°C (77°F), a load per row of 80,000 N (18,000 lb), and a rotational speed of 560 rpm, which corresponds to a train speed of 97 km/h (60 mph). The study concluded that the heat generated in the bearing was proportional to the number of jammed rollers and that the heat generation at the roller-end contacts increased with the number of jammed rollers.

In yet another theoretical work, finite element analysis with ABAQUS and FORTRAN was used to model thermally induced failures in railroad class F ($6\frac{1}{2} \times 12$) tapered-roller bearings, which resulted from laboratory experiments conducted at high operating speeds.[8] The experiments were conducted by the Association of American Railroads (AAR), and showed that new (defect-free) bearings failed after 200 to 300 hours of operation at a speed of 161 km/h (100 mph) and none failed at 129 km/h (80 mph).[8] The study concluded that the thermal and mechanical instabilities in a railroad roller bearing are directly related to the heat generated at the roller-end contacts. The increase in the heat generation is a direct consequence of the grease starvation mechanism caused by the high operating speeds, which results in a larger friction coefficient.[8]

Understanding that manufacturing tolerances of bearing assembly components are hard to maintain on a large-scale production basis, in the 1970's Jamison et al. conducted a detailed study of the geometric effects on the rib-roller contact in tapered-roller bearings,[9] as the latter directly influences bearing performance. As anticipated, their findings indicate that out-of-tolerance components can result in abnormal operating conditions leading to excessive friction and rapid wear at the rib-roller contact region, which can cause roller skew and grease starvation that may eventually lead to catastrophic bearing failure. Consequently, a number of other theoretical and experimental studies have been performed to explore the effects of geometrical imperfections and surface irregularities on the vibrational characteristics of tapered-roller bearings under varying axial loading and rotational speeds[10–12] and to detect bearing defects using frequency domain analysis.[13] Gupta investigated the dynamics of a tapered-roller bearing by modelling the general motion of the roller and cage based on the frictional behaviour and cage clearances of the bearing.[14] His study showed that roller skew (misalignment) increases with increasing friction. At relatively high friction and low cage-pocket and guide-land clearances, the roller was found to maintain steady contact with the cage pocket on one side while the contact is cyclic (pivoting) on the other end. Gupta's findings were later confirmed by an experimental study that was conducted by Yang et al. using specialized capacitance probes to measure and examine the effects of speed and lubrication on the degree of the roller skew (misalignment).[15] It was discovered that the friction between the rib-roller end contact causes the roller's large end (pointing toward the grease seal) to run ahead of the smaller end (pointing toward the spacer ring), thus, leading to roller misalignment. The degree of the roller skew may vary between rollers, and it increases with increasing speed and the lubrication of the larger end of the roller.

Despite the progress made in understanding the dynamics of tapered-roller bearings, no methods or techniques have been developed to identify temperature trending events that result from vibration-induced roller misalignment. Tarawneh et al. conducted a series of experimental and theoretical studies aimed at exploring temperature trending in railroad bearings, finding the root cause of this troubling phenomenon and devising ways to identify it using vibration analysis techniques.[16–22] The authors first set out to replicate the discoloration of tapered rollers (evidence of heating) observed in the trended bearings removed from service.[16] Theoretical modelling agreed with the laboratory testing results in proving that extreme roller temperatures can occur without noticeably raising the temperature of the bearing cup outer surface—the part of the bearing

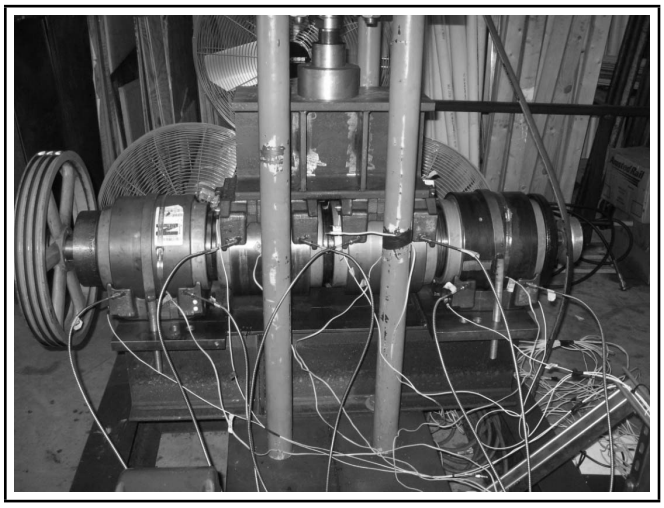

Figure 1. A picture of the four-bearing dynamic tester at UTPA showing the sensor placement.

scanned by the current wayside detectors.[17–19] For example, one of the case studies demonstrated that it is possible for three consecutive rollers within a cone assembly to operate at an abnormal temperature of 232°C (which would cause roller discoloration), yet the bearing cup temperature stays at 88.5°C.

With the new understanding of heat transfer paths of tapered-roller bearings based on experimental and theoretical studies,[17–19] Tarawneh et al. next conducted a series of tests on "trended" bearings pulled from field service along with their mates (the bearing on the opposite end of the axle).[20] The latter work was based on eight laboratory experiments performed on a four-bearing dynamic tester, depicted in Fig. 1, with an axle rotational speed of 536 rpm, which is equivalent to a train traveling at 91.7 km/h (57 mph). One experiment featured a trending event in which the bearing cup temperatures of two bearings experienced a 24°C (43.2°F) increase over a period of 50 minutes.[20] This behaviour occurred simultaneously in a field-trended bearing and its mate, which were separated by a control bearing. The synchronized temperature response ruled out heat transfer as the source for the abrupt change in temperature. The only other explanation for the observed phenomenon is vibration induced heating, where the effects of the oscillations of the rollers in the trended bearing travel along the axle and trigger similar behaviour in the mate bearing. Upon disassembly and inspection, a spall was found on one of the cup raceways of the trended bearing, providing evidence that roller vibration could be the root cause of the temperature trending. Subsequent laboratory tests were effective in achieving temperature trending by using a bearing with a known cup raceway defect to trigger vibration-induced roller misalignment, which is responsible for producing excessive frictional heating in short time periods. The aforementioned laboratory findings were validated in a carefully controlled and executed field test.[21] A bearing in field service, unlike the laboratory setting, is exposed to a variety of vibration excitation sources such as wheel impacts resulting from wheel flats, railcar hunting, and rail track defects. Hence, the performed field test utilized defective wheels as the vibration source to initiate temperature trending in the test bearings. The field test was successful in reproducing several bearing temperature trending events, thus, providing further evidence to verify the laboratory results.[21,22]

The authors used vibration-monitoring techniques to identify dynamics likely associated with roller misalignment and correlate the onset of such dynamics with abrupt changes in bearing temperature. Depending on the relative spacing between the rollers, cage bars and cones, and on the magnitude of the vibration trigger, roller oscillations can be severe and are more likely to lead to rollers being caught misaligned as they enter the loaded region of the bearing. In such cases, the roller's large end will tend to lead due to the friction between the cone rib and the roller end contact point. Consequently, excessive frictional heating will be generated as the severity and number of misaligned rollers increases. The latter will manifest in a sudden rise in bearing-cup temperature. Friction created by sliding misaligned rollers will reduce the epicyclical speed of the cage, which may also vary based on the severity and number of misaligned rollers. In the presence of misalignment, a roller will occupy more space within the cage pocket causing deformations of the cage and essentially creating a tighter fit throughout the cone assembly. Hence, it is expected that the occurrence of roller misalignment will effectively decrease the level of vibration within a bearing as rollers no longer roll or have space to oscillate within the cage pockets.

Roller realignment can occur for one of many reasons including thermal expansion in the cone assembly components, grease circulation, external vibration sources, etc. During the realignment process, a roller will pivot within the cage pocket as the cage and radial clearance reduces forcing rollers to realign. This behaviour is similar to the investigations conducted by Gupta in which one end of the roller maintains steady contact with one side of the cage pocket while the other end pivots.[14] In this scenario, the constant pivoting interaction between the roller and raceway surfaces may explain why defects tend to generally develop on raceways anywhere between the centre of the roller and the smaller end. The pivoting motion, while detrimental to a bearing's life, may promote grease flow, decreasing the temperature to or below normal operating conditions. The cyclic behaviour of the roller will affect the rotational frequency of the cage, momentarily speeding up or slowing down depending on the location and impact of the roller within the cage pocket. Overall, the vibration levels are expected to increase due to the pivoting motion of the roller. Hence, it is essential to quantify the total vibration energy of a bearing in order to garner vital information regarding its operating condition.

It has been experimentally observed that a bearing operating at normal conditions maintains a steady level of vibration energy with minor fluctuations. However, a bearing's vibration energy tends to decrease shortly prior to an increase in temperature and will increase prior to a drop in temperature. This observation proposes a relationship between vibration energy, roller misalignment, and temperature trending events.

The work presented in this paper differs from others in that it focuses on relating the temperature and vibration energy characteristics of a bearing experiencing a temperature trending event in an effort to devise an algorithm that can be used to differentiate between defective bearings nearing the end of their service life and defect-free bearings exhibiting a trending event. To this end, the following methodology was utilized to meet the objectives of this study:

1. The bearing components' fundamental frequencies were determined from a two-dimensional kinematic model.[21,22]

2. A Fast Fourier Transform (FFT) of the acquired data was performed to identify potential shifts in the fundamental frequency of the cage and its harmonics.

3. The total vibration energy was determined by calculating the area under the Power Spectral Density (PSD) curve.

4. Abrupt bearing heating caused by roller misalignment is demonstrated through:

   (a) a reduction in the vibration energy levels within the bearing as misaligned rollers tend to deform the cage, thus, creating a tighter fit between bearing components, and

   (b) a decrease in the rotational frequency of the cage and its overtones due to the excessive friction generated by the sliding rollers at the cone rib and roller end contact.

5. Subsequent decrease in bearing-cup temperature is confirmed through:

   (a) an increase in the vibration energy level as the cage and radial clearance reduction forces rollers to pivot within the cage pocket in an attempt to realign, and

   (b) an increase in the rotational frequency of the cage and its harmonics coupled with some fluctuations due to the pivoting motion of the rollers within the cage pockets.

6. Demonstrate the effects of vibration on temperature by proving that changes in vibration energy precede sudden changes in temperature.

3. EXPERIMENTAL METHODOLOGY

The experiments were performed using two-dynamic bearing testers. A picture of one of these testers showing the experimental setup and sensor locations is provided in Fig. 1. Each dynamic tester can accommodate four class F ($6^1/_2 \times 12$), class K ($6^1/_2 \times 9$), class E (6×11), or class G (7×12) tapered-roller bearings mounted on a customized axle. The first tester employs an 18.64 kW (25 hp) fixed-speed motor with a pulley-drive system. Four distinct pulley sizes are used to rotate an axle at angular velocities of 498 rpm, 562 rpm, 618 rpm, and 796 rpm, which correspond to train speeds of 85.30 km/h (53 mph), 96.56 km/h (60 mph), 106.2 km/h (66 mph), and 138.40 km/h (86 mph), respectively. The second tester utilizes a 22 kW (30 hp) variable-speed drive motor managed by a smart controller that can produce equivalent train speeds ranging from ∼5–138 km/h (∼8–86 mph). Forced convection cooling over the axle-bearing assembly is achieved with three fans that produce an average air stream of 5 m/s (11.2 mph). Each dynamic bearing tester is equipped with a hydraulic cylinder capable of applying vertical loads ranging from 0 to 150% of a full-operating load [100% load condition simulates a fully-loaded freight car and corresponds to a load of 159,000 N (35,750 lb per bearing) for class F and class K bearings, 122,326 N (27,500 lb per bearing) for class E bearings, and 178,000 N (40,000 lb per bearing) for class G bearings].

The dynamic bearing tester with the variable-speed drive motor is housed in a specially constructed temperature-controlled environmental chamber capable of maintaining a wide range of ambient temperatures from as low as $-40°$C ($-40°$F) and up to 55°C (131°F). The environmental chamber is equipped with a commercial freezer unit with a cooling capacity of 7.6 kW. An added feature of the chamber tester is the ability of the smart controller to output the axle torque, speed, and motor power consumption with an accuracy of $\pm 0.5\%$.

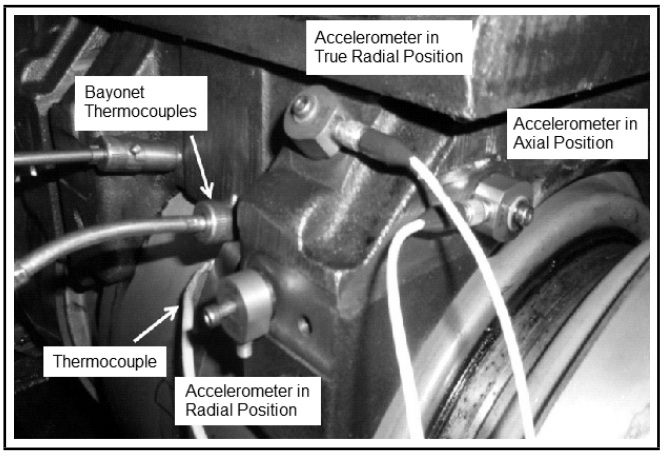

Figure 2. Thermocouple and accelerometer sensor placement.

The bearing adapters are specifically machined to accommodate two accelerometers and two K-type bayonet thermocouples—one on each raceway. The vibration sensors used are single-axis through-hole mount accelerometers with a sensitivity of 10 mV/g, a peak measuring range of ± 500 g, and a bandwidth of 10 kHz. Two accelerometers were placed either on the pulley or odometer side of an adapter. One accelerometer was located on the side face of the adapter (referred to as the axially-mounted accelerometer). The second accelerometer was placed either on the back face or on the edge slant of the adapter, corresponding to radial and true radial placement, respectively. To verify the accuracy of the bayonet thermocouples, a K-type thermocouple was secured to the centre of the bearing cup using a hose clamp and aligned with the bayonet thermocouples. Two additional K-type thermocouples were placed on the front and back of the test rig to record the ambient temperature. A total of fourteen thermocouples and eight accelerometers were monitored and recorded during testing. Thermocouple and sensor locations are shown in Fig. 2.

For this study, four test speeds ranging from low to high were chosen: 233 rpm, 498 rpm, 560 rpm, and 796 rpm, which are equivalent to train-traveling speeds of 40.23 km/h (25 mph), 85.30 km/h (53 mph), 96.56 km/h (60 mph), and 138.40 km/h (86 mph), respectively. Only class F and K bearings were used for all the experiments discussed in this paper.

The experimental setup was designed to replicate speeds and cargo loads observed in field service. Depending on the specific test conducted, a "trigger" bearing with a known cup raceway defect (i.e., a cup spall) was used to introduce vibration into the axle-bearing assembly in order to promote roller misalignment. The cup spalls utilized in the laboratory testing were either spalls that developed naturally in service and were pulled from the field or artificially-made spalls created in the laboratory by grinding off material from the cup raceway. A picture of one of the naturally-spalled cup raceways used in the laboratory testing can be seen in Fig. 3.

The four bearings mounted on the customized axle were labelled as Bearings 1 through 4 starting at the pulley side. Four tests were conducted for each experiment that utilized a trigger bearing. Referring to Fig. 4, in the first three tests, the location of the cup spall was varied between 345° (just before the load

Figure 3. Cup raceway spall that developed naturally in service and was pulled from the field.

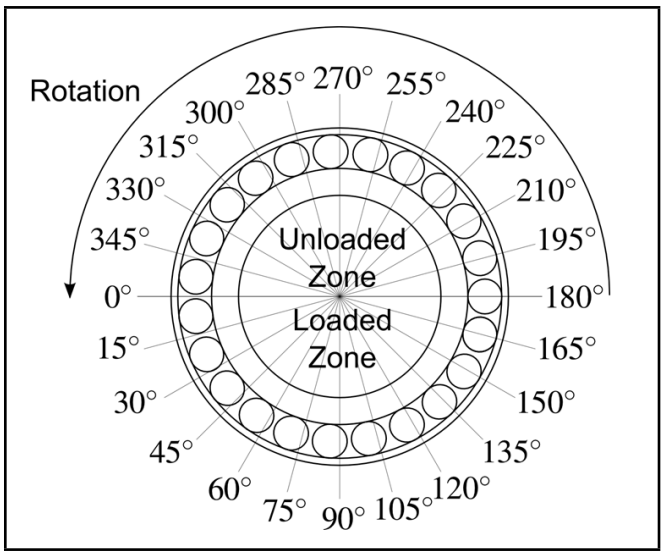

Figure 4. Spall placement diagram for bottom-loaded bearings (inverted for top-loaded bearings).

zone), 0° (at the beginning of the load zone), and 15° (just after the beginning of the load zone); all run at a 17% load simulating an empty railcar. The test generating the most temperature trending events was repeated utilizing a 100% load simulating a fully-loaded railcar, which constituted the fourth and last test of the experiment. A discussion of the data analysis techniques used to acquire the results of this study follows.

4. DATA ANALYSIS

The temperature data was recorded once every 20 seconds, utilizing a sampling rate of 100 samples per second. Hence, each temperature data point is the average of 100 readings. Furthermore, the bearing temperature profiles were generated by averaging the readings of the two K-type Bayonet thermocouples that monitor the temperature of the two raceways within each bearing.

The vibration data was sampled at a rate of 9600 samples per second or 10240 samples per second depending on the data acquisition system used. Due to data storage limitations associated with the prolonged durations of these tests, the data acquisition systems were programmed to record 20 seconds of data and generate a file once every 10 minutes. The raw data file contained the time and acceleration (g) recorded by each accelerometer used during testing. The frequency response was generated by performing an ensemble average of

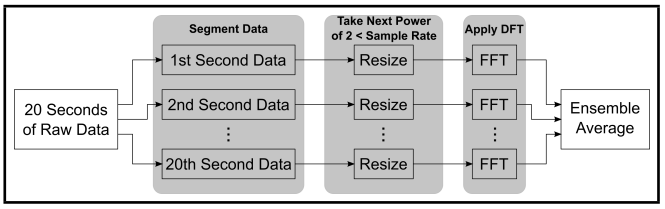

Figure 5. Ensemble averaging process.

twenty, one-second segments of data collected at a constant axle speed (i.e., twenty seconds of raw vibration data was partitioned into one-second intervals). Hence, each one-second segment contained either 9600 or 10240 samples. The discrete Fourier transform (DFT) was calculated for each segment using a MATLAB™ fast Fourier transform function (FFT). The MATLAB™ fast Fourier transform functions are based on a library called FFTW.[23,24] They can be used to compute N-point DFTs. Because the numerical method employed performs fastest when N is power of 2, for each one-second segment, 8192 samples are used to generate the DFT where 8192 is the next power of 2 less than either 9600 or 10240. The mean of the resulting twenty DFTs is then taken to generate the ensemble average. The process described here is illustrated in Fig. 5. For analysis purposes, the resulting amplitude spectrum is plotted up to the Nyquist frequency so that the frequency range is from 0 to half the power of 2 less than the sampling rate (i.e., 0 to 4096 Hz). Note that doubling the sampling rate did not change any of the results or conclusions presented in this study.

In order to identify the level of vibration in a bearing, the *direct approach* was used in order to evaluate the energy contained in an analogue signal, $x(t)$, as the magnitude of a signal squared integrated over time, as shown by Eq. (1),

$$E = \int_{-\infty}^{\infty} |x(t)|^2 dt. \tag{1}$$

Furthermore, from Parseval's Theorem, which states that

$$\int_{-\infty}^{\infty} |x(t)|^2 dt = \int_{-\infty}^{\infty} |X(f)|^2 df; \tag{2}$$

it can be shown that the energy density function, $|X(f)|^2$, referred to as the energy spectral density, the power spectral density (PSD), or simply the power spectrum (PS), integrated over the frequency range is equal to the energy contained in a signal. In the direct approach, the power spectrum is calculated as the magnitude squared of the Fourier transform, as shown in Eq. (3),

$$PS(f) = |X(f)|^2. \tag{3}$$

The use of Eqs. (1)–(3) allows for a simple manipulation to measure the energy of a signal by determining the power spectrum and integrating over a specified range of frequencies.

Frequency analysis facilitated identification of the bearing components' primary frequencies. There are a total of six fundamental frequencies observed in tapered-roller bearings. All frequencies are dependent on the rotational frequency of the axle (ω_o). Three of the bearing component angular frequencies are the cone (ω_{cone}), the cage (ω_{cage}), and the roller (ω_{roller}) frequencies. The remaining three frequencies correspond to defects or geometrical irregularities on the cup (outer) raceway

Table 1. Bearing manufacturer class F / K specified cone dimensions.

D_{cone} [cm]	18.887
L_{cone} [cm]	5.034
Φ_{cone} [rad]	0.141

Table 2. Bearing manufacturer class F / K specified roller dimensions.

D_{l} [cm]	2.223
D_{s} [cm]	2.057
Θ_{roller} [rad]	0.033

(ω_{out}), the cone (inner) raceway (ω_{in}), and the roller (ω_{rolldef}). These frequencies tend to increase in magnitude when an associated defect or geometric inconsistency is present. Dimensions of the cone and roller as specified by the manufacturer, given in Table 1 and Table 2, respectively, were used to calculate the dimensions necessary to derive the fundamental frequencies. The mean diameter of a tapered roller, d_{roller}, is calculated along its centre. The radius of the cone, r_{cone}, is calculated from the centre of the cone to the centre of the raceway also known as the centre of the tapered length. The radius of the cup, r_{cup}, is calculated as the distance between the centre of the cone and the location where the mean diameter of the roller, d_{roller}, comes in contact with the cup raceway. A cross-sectional diagram of a railroad bearing illustrating the locations of the abovementioned measurements is provided in Fig. 6. Final dimensions used to calculate the bearing components primary frequencies are listed in Table 3.

The equations used to obtain d_{roller}, r_{cone}, and r_{cup} utilizing information presented in Table 1 and Table 2 are provided hereafter as Eqs. (4–6):

$$d_{\text{roller}} = \frac{D_{\text{l}} + D_{\text{s}}}{2}; \tag{4}$$

$$r_{\text{cone}} = \frac{d_{\text{cone}}}{2} - \frac{L_{\text{cone}}}{2}\sin(\phi); \tag{5}$$

$$r_{\text{cup}} = r_{\text{cone}} + d_{\text{roller}}\cos(\phi + \theta). \tag{6}$$

The equations used to determine the six fundamental frequencies of tapered-roller bearings, Eqs. (7–12), were derived by Tarawneh et al. from a 2-D kinematic model.[21,22] Detailed derivations of these equations can be found elsewhere.[25]

$$\omega_{\text{cone}} = \omega_{\text{o}}; \tag{7}$$

$$\omega_{\text{cage}} = \left(\frac{r_{\text{cone}}}{r_{\text{cone}} + r_{\text{cup}}}\right)\omega_{\text{cone}}; \tag{8}$$

$$\omega_{\text{roller}} = \left(\frac{r_{\text{cone}}}{d_{\text{roller}}}\right)\omega_{\text{cone}}; \tag{9}$$

$$\omega_{\text{out}} = 23\,\omega_{\text{cage}}; \tag{10}$$

$$\omega_{\text{in}} = 23\,(\omega_{\text{cone}} - \omega_{\text{cage}})\,; \tag{11}$$

$$\omega_{\text{rolldef}} = \left(\frac{r_{\text{cup}}}{d_{\text{roller}}/2}\right)\omega_{\text{cage}}. \tag{12}$$

5. DISCUSSION OF RESULTS

As mentioned earlier in this paper, experimentally acquired data indicate that a bearing operating at normal conditions maintains a steady level of vibration energy with minor fluctuations. However, during temperature trending events brought on by roller-misalignment, the vibration energy tends to decrease shortly prior to an increase in temperature and will increase prior to a drop in temperature. These observations signify that there is a relationship between vibration energy, roller misalignment, and temperature trending events.

Table 3. Class F / K tapered-roller bearing calculated dimensions.

d_{roller} [cm]	2.140
r_{cone} [cm]	9.089
r_{cup} [cm]	11.196

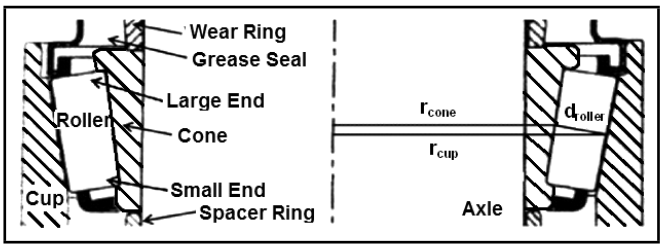

Figure 6. Cross-sectional diagram illustrating the locations of the measurements used to calculate the bearing components fundamental frequencies.

To provide evidence of the abovementioned behaviour, a series of laboratory tests were conducted utilizing several different combinations of operating speed and loading conditions, as described in Table 4. For each experiment, the temperature history and the vibration energy plots were generated. Select instances were then identified just prior to an increase or decrease in the vibration energy levels within a specific bearing on the bearing-axle assembly. The corresponding points on the temperature profile of that specific bearing were also determined, which generally preceded the onset of an abrupt change in temperature. The time delay between the initiation of a vibration energy trend and a temperature trend was tracked and quantified to demonstrate the effects of vibration on the bearing temperature.

The rotational frequencies of the dominant cage harmonic (ω_{out}) were tracked throughout the experimental testing in order to demonstrate the effects of roller-misalignment. Instances in the ω_{out} signal corresponding to an abrupt change in the energy level were identified. A subsequent point in time at the lowest or highest level in energy was chosen to analyse and provide evidence of changes in the rotational speed of the cage. Based on previously performed research,[25] in order to account for slip, the experimentally acquired ω_{out} rotational frequencies were determined by selecting the dominant frequency within ± 1 Hz for speeds less than 600 rpm and ± 1.5 Hz for speeds greater than 600 rpm of the theoretically calculated frequency given by Eq. (10). Note that the figures in this paper display the dominant ω_{out} frequency within the range and ignore the sideband peaks that may result from roller misalignment. Table 5 provides the six theoretically calculated fundamental bearing component frequencies, Eqs. (7–12), based on the utilized test speeds.

Table 4. Experimental setup description.

Experiment	Load	Speed [km/h] (mph)	Spall [°]	Bearing 1	Bearing 2	Bearing 3	Bearing 4
1	17%	96.56 (60)	345	Normal Poly	Normal Poly	Normal Poly	Steel Trigger
2	17%	96.56 (60)	10	Normal Poly	Normal Poly	Normal Poly	Steel Trigger
3	100%	85.30 (53)	350	Normal Poly	Normal Steel	Normal Poly	Steel Trigger
4	125%	138.40 (86)	N/A	Normal Poly	Normal Poly	Normal Poly	Normal Poly
5	17%	40.23 (25)	N/A	Normal Poly	Normal Poly	Normal Poly	Normal Poly

Table 5. Class F / K natural frequencies of tapered-roller bearing components and defects.

Natural Frequency [Hz]	40.23 km/h (25 mph) (233 rpm)	85.30 km/h (53 mph) (498 rpm)	96.56 km/h (60 mph) (560 rpm)	138.40 km/h (86 mph) (796 rpm)
ω_{cone}	3.88	8.30	9.22	13.27
ω_{cage}	1.74	3.72	4.13	5.94
ω_{roller}	16.49	35.25	39.15	56.35
ω_{out}	40.02	85.53	94.98	136.72
ω_{in}	49.30	105.37	117.00	168.42
$\omega_{rolldef}$	18.21	38.92	43.21	62.20

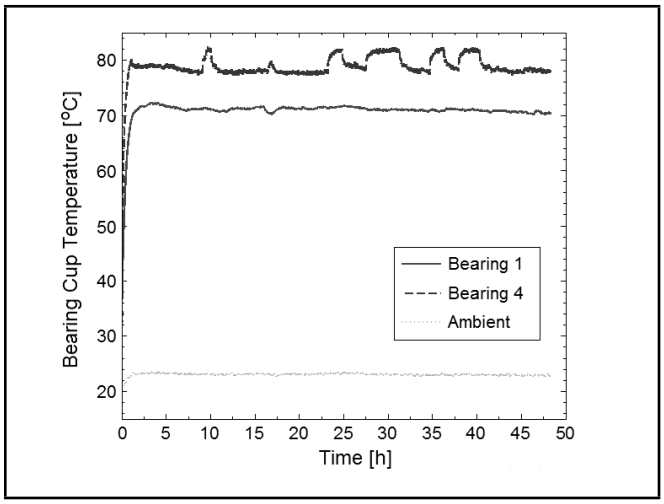

Figure 7. Experiment 1 bearing temperature profiles; class K bearings; spall placement: 345° (refer to Fig. 4); speed: 96.56 km/h (60 mph); load: 17% (empty railcar).

5.1. Experimental Results

5.1.1. Experiment 1

Experiment 1 was carried out at a speed of 95.56 km/h (60 mph, 560 rpm) and a load of 17%, simulating an unloaded railcar. A cup spall on Bearing 4 positioned 15 degrees before the load zone (345° referring to Fig. 4) provided the vibration source for the axle-bearing assembly. The temperature profiles and bearing vibration energies can be seen in Fig. 7 and Fig. 8, respectively. Bearing 4, a bottom-loaded bearing with a spalled cup, displayed multiple fluctuations in temperature. At five different instances, the temperature increased and held steady at approximately the same level before returning to normal operating conditions. The temperature profile for Bearing 4 along with the corresponding vibration energy recorded by the accelerometer is provided in Fig. 9. It can be seen that each increase in temperature is preceded by a decrease in the vibration energy level. The aforementioned phenomenon seems to suggest that roller misalignment, which is what causes the decrease in the vibration energy of the bearing, is also what generates the frictional heating that eventually results in the observed rise in temperature. Note that the vibration energy decreased to similar levels at each of the corresponding five temperature increases.

To further illustrate the abovementioned observations, four select data points were examined—two uptrends and two downtrends. Referring to Fig. 9, energy began to decrease significantly at approximately 8.83 and 34.5 hours into the test. Consequently, the temperature began to increase at approximately 9.08 and 34.68 hours into testing. In each case, vibration energy changes preceded temperature changes by 10.8 to 15 minutes. Conversely, increases in vibration energy occurring at approximately 24.67 and 40.17 hours into the test preceded decreases in temperature observed at 24.79 and 40.27 hours into the test, respectively. Again, changes in temperature lagged those in vibration energy by 6 to 7.2 minutes. The latter behaviour cannot be explained by changes in lubrication nor thermal expansions of bearing components. The short period between vibration activity and temperature reaction provides supporting evidence that this phenomenon is the result of bearing heating brought on by vibration-induced roller misalignment. Note that, even though the remaining three bearings on the axle displayed changes in their vibration energy similar to Bearing 4, the magnitude of these changes was much smaller, as seen in Fig. 8, and did not result in an increase in the bearing temperature. The latter behaviour can be explained by *cross-talk* between the four bearings that share an axle. Given the fact that Bearing 4 has a significant spall on its outer (cup) raceway, the generated vibration will be picked up by the remaining three bearings, and so do any noticeable changes in that vibration energy. However, since the rollers are not actually misaligned on those other three bearings, no change in temperature accompanies the observed changes in vibration.

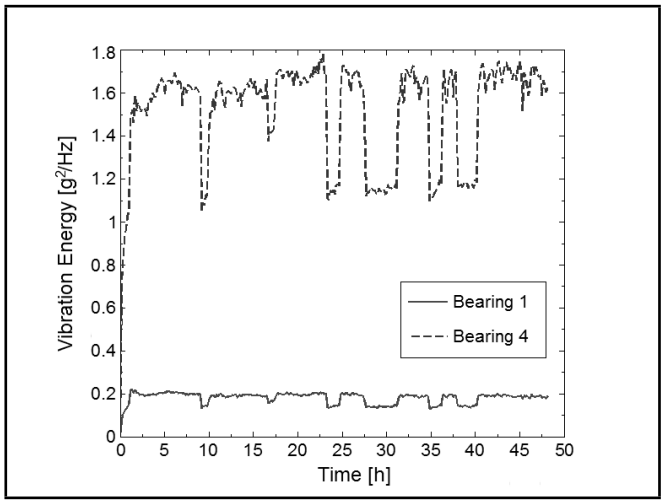

Figure 8. Experiment 1 vibration energy captured by radial accelerometers.

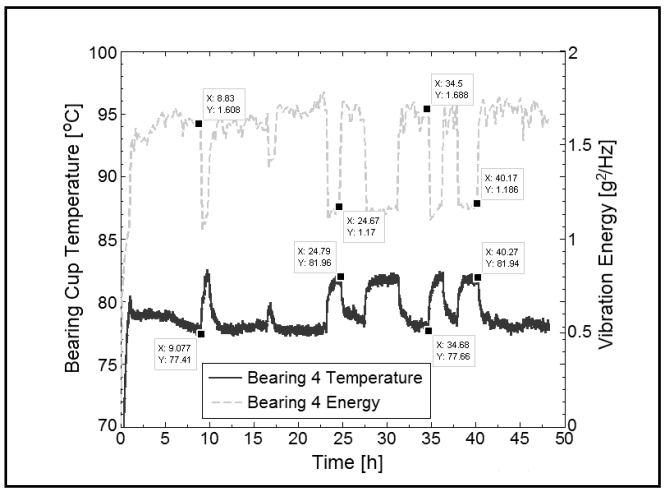

Figure 9. Experiment 1 temperature profile vs. vibration energy for Bearing 4.

In accordance with the hypothesis proposed in this paper, the pivoting motion of a roller can either speed up or decrease the rotational speed of the cage. In order to identify potential shifts in frequency, the total vibration energy of Bearing 4 was plotted alongside the fundamental ω_{out} frequency, as shown in

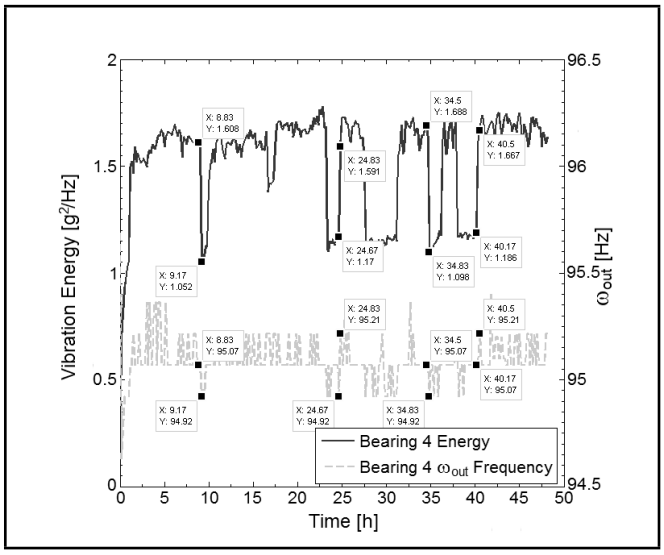

Figure 10. Experiment 1 vibration energy vs. the fundamental ω_{out} frequency for Bearing 4.

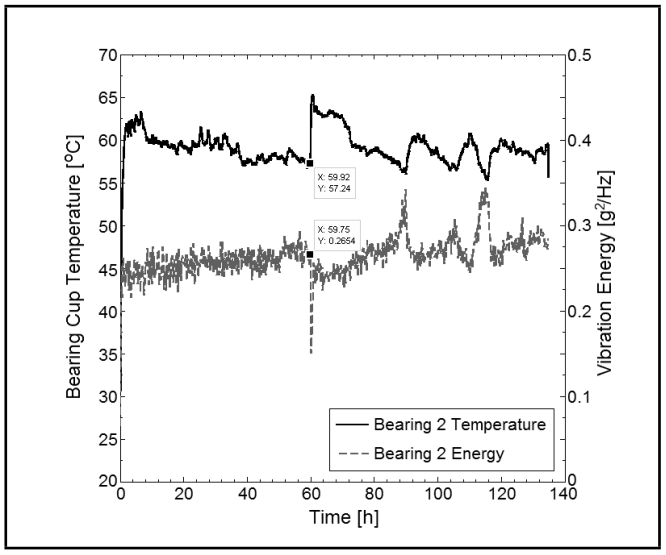

Figure 11. Experiment 2 bearing temperature vs. vibration energy; class F bearings; spall placement: 10° (refer to Fig. 4); speed: 96.56 km/h (60 mph); load: 17% (empty railcar).

Fig. 10. The ω_{out} frequency at the previously selected four data points in the vibration energy (signifying the start of an increase or decrease in temperature) were compared to the next lowest or highest vibration data point available. Referring to Fig. 10, the two data points examined at 8.83 and 34.50 hours into the test occurred prior to a sudden decrease in vibration energy at 9.17 and 34.83 hours, respectively. In both cases, the frequency ω_{out} decreased from 95.07 to 94.92 Hz. Conversely, the two points selected at 24.67 and 40.17 hours into the test took place approximately 10 to 20 minutes prior to an increase in the vibration energy. An increase in the ω_{out} frequency from 94.92 to 95.21 Hz was observed from 24.67 to 24.83 hours. At 40.17 hours, ω_{out} increased from 95.07 to 95.21 Hz within 19.8 minutes. Hence, Fig. 10 demonstrates the shift to lower frequencies (i.e., slowing down) during a temperature uptrend, and a shift to higher frequencies (i.e., speeding up) during a temperature downtrend. The aforementioned is further validation that vibration-induced roller-misalignment is responsible for the temperature trending phenomenon seen in field service.

5.1.2. Experiment 2

Experiment 2 was performed at a speed of 95.56 km/h (60 mph, 560 rpm) with a 17% load (empty railcar) and a cup spall on Bearing 4 positioned 10 degrees into the load zone (10° referring to Fig. 4). Bearing 2, a class F defect-free top-loaded bearing, experienced a sharp rise in temperature approximately 60 hours into the test, as can be seen in Fig. 11. To demonstrate the effects of vibration on temperature, the temperature profile for Bearing 2 is juxtaposed in Fig. 11 with the corresponding vibration energy. The vibration energy exhibited a significant decrease moments prior to the abrupt increase in temperature. The vibration energy for Bearing 2 began to drop dramatically at approximately 59.75 hours into the test, which was followed by a rapid rise in temperature that started at approximately 59.92 hours (10.2 minutes later). Again, the most likely explanation for the decrease in the vibration energy of Bearing 2 is roller-misalignment which causes frictional heating resulting from metal-to-metal contact (i.e., rollers sliding on the bearing raceways rather than rolling). The short period between the initial decrease in vibration energy and the onset of the sharp increase in the temperature of Bearing 2 seems to suggest a multiple-roller misalignment, which can generate significant heating in short time periods.[19] Note that, unlike the previous case of a defective trended bearing, the sudden change in energy at approximately 60 hours into the test did not affect the vibration energy of the other three bearings on the axle.

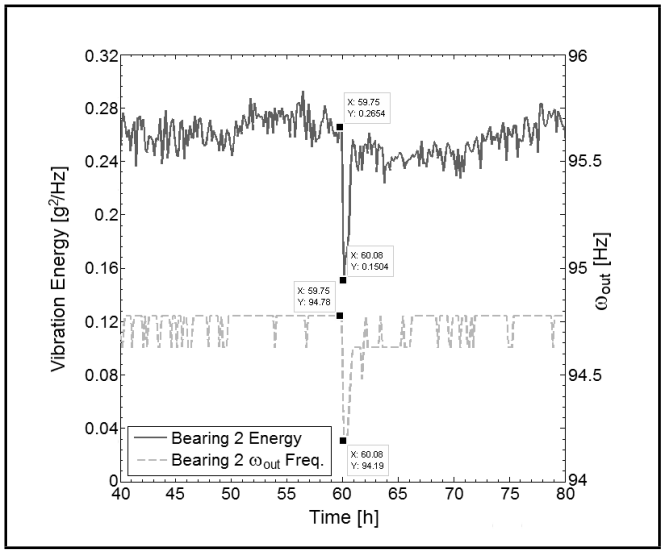

Figure 12. Experiment 2 vibration energy vs. the fundamental ω_{out} frequency for Bearing 2.

The fundamental ω_{out} frequency for Bearing 2 is plotted in Fig. 12 alongside the vibration energy acquired using the radial accelerometer. It can be seen from Fig. 12 that the major drop in vibration energy observed between 59.75 and 60.08 hours is accompanied by a significant drop in the ω_{out} frequency, which decreased from 94.78 Hz to 94.19 Hz during that 20-minute interval. Although there were many small fluctuations in the rotational frequency of ω_{out}, none were as big or accompanied by as sharp of an increase in temperature as the one occurring at 59.75 hours. A drop in the ω_{out} rotational frequency of approximately 0.6 Hz suggests a multiple-roller misalignment scenario, which explains the abrupt increase in bearing temperature and decrease in the vibration energy caused by the rollers sliding on the raceways.

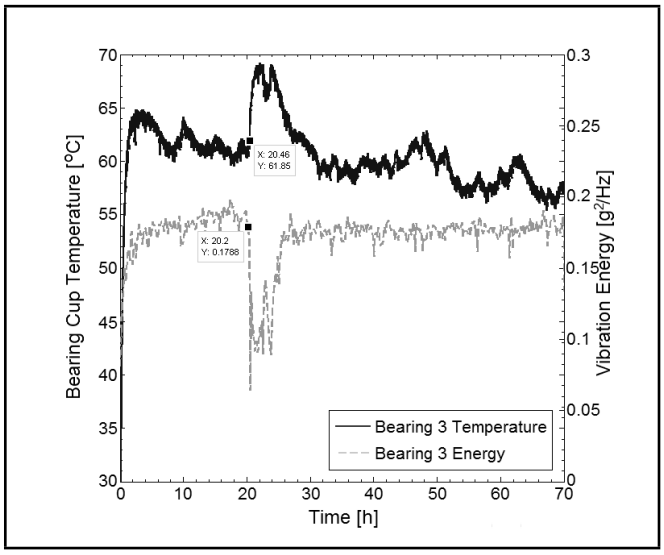

Figure 13. Experiment 3 bearing temperature vs. vibration energy; class F bearings; spall placement: 350° (refer to Fig. 4); speed: 85.30 km/h (53 mph); load: 100% (fully-loaded railcar).

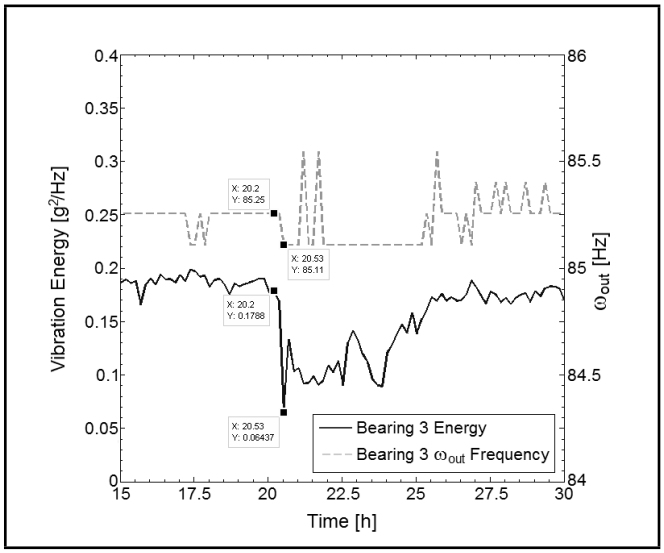

Figure 14. Experiment 3 vibration energy vs. the fundamental ω_{out} frequency for Bearing 3.

5.1.3. Experiment 3

Experiment 3 was conducted at a speed of 85.30 km/h (53 mph, 498 rpm) with a 100% load (simulating a fully-loaded railcar) and a cup spall on Bearing 4 positioned 10 degrees before the start of the load zone (350° referring to Fig. 4). As in Experiment 2, Bearing 3, a class F defect-free top-loaded bearing, exhibited a rapid increase in temperature approximately 20 hours into the test, as seen in Fig. 13. To exemplify the effects of vibration on temperature, the temperature profile for Bearing 3 is juxtaposed in Fig. 13 with the corresponding vibration energy of that bearing. It can be observed that the energy began to decrease markedly at approximately 20.2 hours into the test, which was then followed by a sharp increase in the bearing temperature that initiated at 20.46 hours (15.6 minutes later). The temperature response time lag can be explained by the thermal time constant of tapered-roller bearings. It takes some time for the bearing cup, where the temperature is being measured, to sense the effects of the frictional heating caused by roller-misalignment and slipping. Depending on the degree of roller-misalignment and the number of rollers that are caught misaligned, the amount of frictional heating produced within the bearing can vary dramatically.[7,19] The latter accounts for the variations seen in the thermal time constant of the bearing, which can range anywhere from about one minute and up to 25 minutes depending on the severity of roller-misalignment and the number of jammed rollers. Note that the temperature trending experienced by Bearing 3 (a defect-free bearing) did not have any noticeable effect on the vibration energy of the other three bearings on the axle.

The primary ω_{out} frequency for Bearing 3 is presented in Fig. 14 next to the vibration energy measured by the radial accelerometer. A drop in the vibration energy of the bearing is observed from 20.2 hours to 20.53 hours into the test. During that period, the ω_{out} frequency decreased from 85.25 Hz to 85.11 Hz suggesting a slight decrease in the rotational speed of the roller-cage brought on by roller misalignment. The figure also shows that the decrease in the ω_{out} frequency persists throughout the period in which the total vibration energy experiences a downtrend (i.e., between 20 and 25.5 hours in the test), which is indicative of consistent roller-misalignment during that time period. As soon as the vibration energy of the bearing begins to rise again, indicating a return to normal operation of rolling without skidding, the temperature of the bearing starts to drop again.

5.1.4. Experiment 4

Experiment 4 is an accelerated class K lifetime test carried out at a speed of 138.40 km/h (86 mph, 796 rpm) with 125% of full-load (simulating an overloaded railcar). All the bearings used in this test were healthy bearings with no known defects. The temperature profiles and bearing vibration energies are presented in Fig. 15 and Fig. 16, respectively. The two outer bearings of the axle-bearing assembly, Bearings 1 and 4, exhibited a noticeable drop in their vibration energy moments before they experienced an abrupt increase in their temperature. The latter suggests a synchronized roller-misalignment event.

Looking at Fig. 17, in which the temperature profile of Bearing 4 is juxtaposed with the corresponding vibration energy, one can notice that the energy began to decrease at approximately 273.5 hours into the test, which was then followed by a sudden increase in the bearing temperature observed at 273.8 hours (i.e., 18 minutes later). Moreover, at approximately 317.3 hours into the test, the vibration energy of Bearing 4 started to increase, which was closely followed by a decrease in temperature at about 317.5 hours (i.e., 12 minutes later). In fact, Fig. 17 clearly demonstrates that each increase in bearing temperature is preceded by a decrease in the vibration energy of the bearing, including the small temperature fluctuation that occurred around 322.5 hours into the test.

The detection of slip caused by roller misalignment is easier to identify in an experiment running at high speeds and loads. Increasing the applied load on bearings decreases the radial clearance, which creates better contact between the roller and the cone and cup raceways. Operating at high speeds and loads tends to increase the bearing temperature, which in turn reduces the viscosity of the grease and shrinks the elastohydrodynamic (EHD) lubricant film that exists between the rolling surfaces. In extreme conditions, grease starvation can occur, which leads to significant roller slipping that results in metal-to-metal frictional heating. As demonstrated earlier, changes

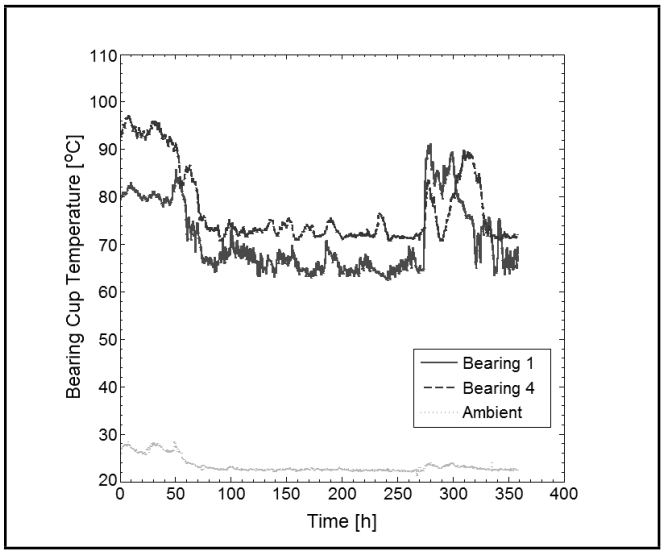

Figure 15. Experiment 4 bearing temperature profiles; defect-free class K bearings; speed: 138.40 km/h (86 mph); load: 125% (overloaded railcar).

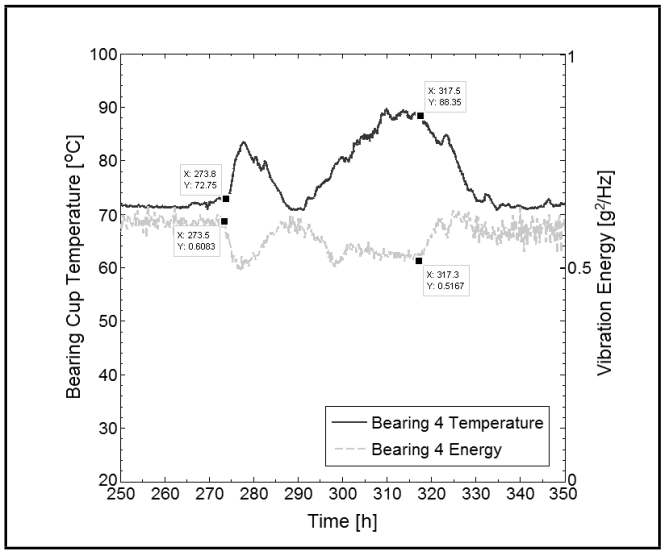

Figure 17. Experiment 4 temperature profile vs. vibration energy for Bearing 4.

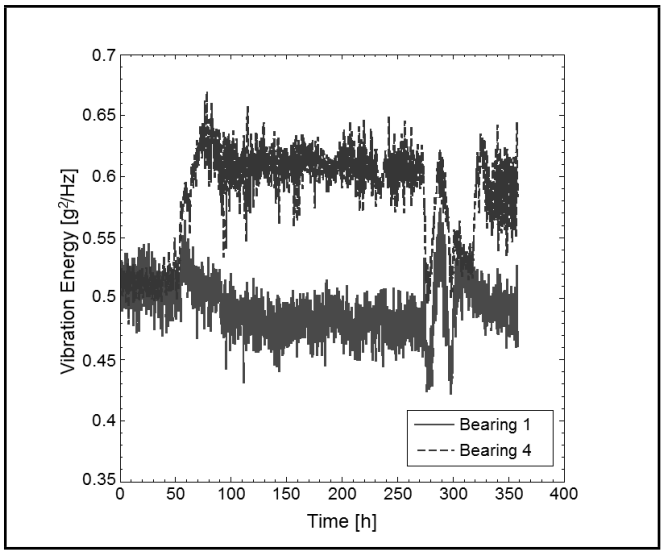

Figure 16. Experiment 4 vibration energy captured by radial accelerometers.

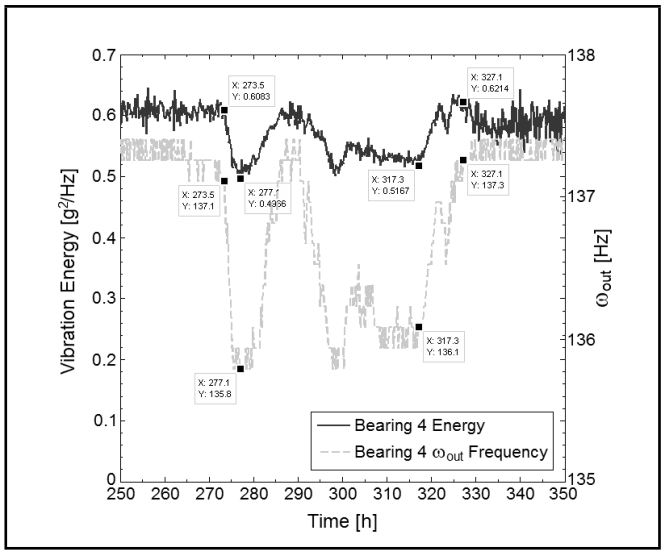

Figure 18. Experiment 4 vibration energy vs. the fundamental ω_{out} frequency for Bearing 4.

in vibration energy within the bearing precede those in temperature. The decrease in the vibration energy within the bearing is attributed to roller slipping which is demonstrated by a decrease in the fundamental ω_{out} frequency. Looking at Fig. 18, a significant decrease of 1.3 Hz is observed in the ω_{out} frequency over the period between 273.5 hours and 277.1 hours into the test, which corresponds to the time the vibration energy of the bearing reaches its lowest value. The figure also illustrates how the ω_{out} frequency closely mimics the trends exhibited by the vibration energy of the bearing throughout the test. Note that, as soon as the bearing vibration energy returns to normal operation levels (indicating rolling without slipping), so does the ω_{out} frequency and the bearing operating temperature.

5.1.5. Experiment 5

Experiment 5 was performed at sub-zero ($-22.5°$C) ambient temperature conditions utilizing the bearing dynamic tester housed in the environmental chamber. Four class K healthy (defect-free) bearings were used in this test and were run at a speed of 40.23 km/h (25 mph, 233 rpm) under 17% load simulating an empty railcar. The bearing temperature histories along with the motor power consumption during the test are provided in Fig. 19, and the corresponding vibration energy plots are given in Fig. 20. The latter two figures provide yet one more example that validates the hypothesis proposed in this paper.

At very low operating temperatures, such as those experienced by the bearings in this experiment, the lubricating grease is very viscous (thick) and creates resistance to the rolling motion, preventing the rollers from normal operation and causing them to misalign and skid along the raceways. Looking at Fig. 20, it can be observed that the grease-induced roller misalignment produces the same effects as the vibration-induced roller misalignment. Whenever roller-misalignment occurs, the vibration energy of the bearing decreases as a result of the reduced epicyclical speed, which is then followed by an increase in the temperature of the bearing resulting from the frictional heating generated by skidding of the roller(s) on the raceways. As the bearing heats, the grease becomes less viscous in the vicinity of the skidding roller(s), thus, allowing the rollers to return to normal operation, which is indicated by the observed increase in the vibration energy of the bearing.

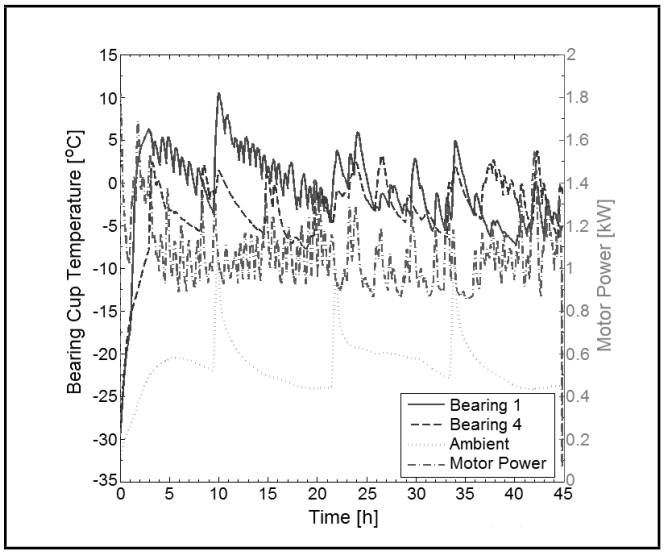

Figure 19. Experiment 5 bearing temperature profiles vs. motor power; defect-free class K bearings; freezing ambient conditions; speed: 40.23 km/h (25 mph), load: 17% (empty railcar).

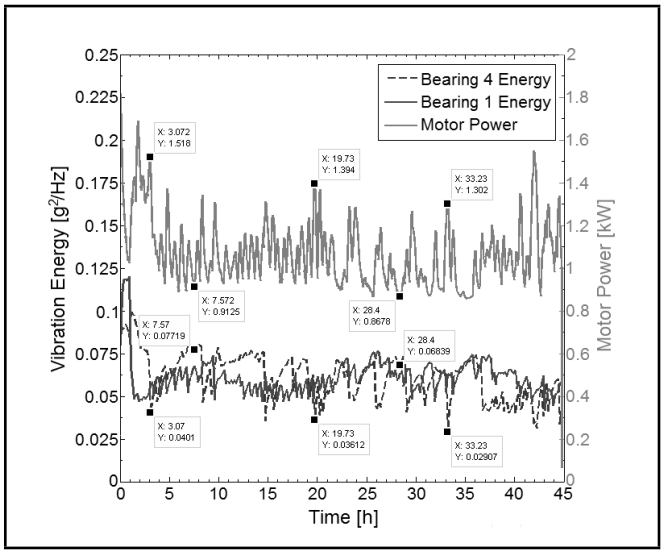

Figure 20. Experiment 5 vibration energy captured by radial accelerometers vs. motor power.

The motor power profile, seen in Fig. 19 and more clearly in Fig. 20, supports the abovementioned observations as the power consumption is found to increase prior to a rise in temperature and drops just before the bearing temperatures start decreasing. The increase in power consumption is expected as the motor (which is managed by a smart controller) is trying to overcome the resistance to the rolling motion caused by the roller-misalignment in an attempt to maintain the axle rotational speed within $\pm 0.5\%$. As soon as the rollers return to normal operating conditions, the motor power drops, which is then followed by a decrease in the bearing temperatures. Further proof is found in Fig. 20, which illustrates that instances of maximum motor power consumption correspond to instances of minimum vibration energy and vice versa. Note that the abrupt changes in ambient temperature, seen in Fig. 19, are caused by the commercial freezer unit defrost cycle which commences every 10 to 15 hours.

6. CONCLUSIONS

The ability to differentiate between defective (faulty) bearings and defect-free (healthy) bearings that are undergoing a temperature trending event is of utmost importance to the railroad industry as this will significantly reduce the number of unnecessary, and very costly, train stoppages associated with *non-verified* bearing removals and/or inspections. This study presents an experimentally validated technique that utilizes the vibration energy approach to identify and differentiate the temperature trending phenomenon exhibited by some defect-free (healthy) bearings in field service.

The technique is built on the hypothesis that, during a bearing temperature-trending event, the vibration energy will decrease prior to a temperature uptrend and will start increasing moments before a temperature downtrend. The aforementioned behaviour is triggered by vibration-induced roller-misalignment. Misaligned roller(s) will slide on the raceways and create a tighter fit between bearing components, thus, slowing the epicyclical speed and producing less vibration than that of pure rolling motion. Meanwhile, the roller-skidding will generate excessive metal-to-metal frictional heating caused by thinning of the elastohydrodynamic (EHD) lubricant film, which accounts for the observed rise in bearing temperature. Once the roller(s) return to normal operation, the vibration energy of the bearing will increase back to its original level and the bearing temperature will start to drop.

This paper provides sufficient experimental proof to validate the proposed hypothesis. The relationship between vibration energy and temperature is further verified by the shift in the ω_{out} frequency, which is dependent on the fundamental frequency of the cage. A shift to a lower ω_{out} frequency indicates that the rotational frequency of the cage has slowed down from its epicyclical motion due to the friction caused by roller misalignment. A decrease in the bearing temperature or return-to-normal operating temperature would be caused by geometrical thermal expansions and roller realignment. During the reduction in cage pocket and radial clearances, the rollers pivot as they attempt to realign, promoting grease flow and momentarily speeding up and causing fluctuations in the rotational speed of the cage.

The abovementioned behaviour is observed in numerous laboratory experiments, and the technique presented here is consistent in identifying the bearing temperature trending phenomenon. The selected tests discussed in this paper varied from setups containing bearings with known defects that would trigger vibration-induced roller misalignment to experiments conducted with all defect-free bearings run at high speeds and loads or low ambient conditions. Note that roller misalignment is not only triggered by vibrations from neighbouring sources, it can be caused by many factors including inadequate lubrication conditions, grease degradation, loose cone assemblies, high operating speeds and loads, or simply low ambient temperatures that significantly increase the grease viscosity and cause grease-induced roller misalignment.

In the case of a defective (faulty) bearing, the vibration energy levels and the bearing temperature will be noticeably higher than those of normal operation—see Fig. 7 and Fig. 8 and compare the defect-free Bearing 1 to the defective Bearing 4, which contains a spalled cup raceway—and the vibration energy of the bearing will continue to increase as the defect worsens with continued operation. Ongoing work in this area is focused on acquiring vibration signatures at different oper-

ating speeds and loads from a variety of healthy and defective bearings to cover a wide range of defects and abnormal operating conditions. The objective is to create an inclusive vibration energy database library that can be used to contrast defect-free bearings and known bearing cup, cone, cage, and roller defects. The latter work combined with the technique presented in this paper will facilitate the development of a comprehensive bearing condition monitoring algorithm that will contribute to a much improved railway safety while reducing the costly train stoppages and delays associated with false bearing setouts and inspections.

REFERENCES

[1] Karunakaran, S. and Snyder, T. W. Bearing temperature performance in freight cars, *Proceedings of the Bearing Research Symposium sponsored by the AAR Research Program in conjunction with the ASME RTD 2007 Fall Technical Conference*, Chicago, Illinois, September 11–12, (2007).

[2] Anderson, G. B. Acoustic detection of distressed freight car roller bearing, *Proceedings of the 2007 JRCICE Spring Technical Conference*, Pueblo, Colorado, March 13–16, (2007).

[3] Wiley, R. B. and Snyder, T. Technical Report, From ATSI to TDTI: Existing Technologies Analysis and Statistical Review Future Technologies, Transportation Technology Center, Inc. and Union Pacific Railroad, (2011).

[4] Farnfield, N. E. Thermal investigations of roller bearings, *Tribology*, **5** (3), 104, (1972).

[5] Dunnuck, D. L. Steady-state temperature and stack-up force distributions in a railroad roller bearing assembly, M.S. thesis, University of Illinois at Urbana-Champaign, Urbana, Illinois, (1992).

[6] Wang, H. Axle burn-off and stack-up force analyses of a railroad roller bearing using the finite element method, Ph.D. dissertation, University of Illinois at Urbana-Champaign, Urbana, Illinois, (1996).

[7] Wang, S., Cusano, C., and Conry, T. F. A dynamic model of the torque and heat generation rate in tapered roller bearings under excessive sliding conditions, *Tribology Transactions*, **36** (4), 513–524, (1993).

[8] Kletzli, D. B., Cusano, C., and Conry, T. F. Thermally induced failures in railroad tapered roller bearings, *Tribology Transactions*, **42** (4), 824–832, (1999).

[9] Jamison, W. E., Kauzlarich, J. J., and Mochel, E. V. Geometric effects on the rib-roller contact in tapered roller bearings, *ASLE Transactions*, **20** (1), 79–88, (1977).

[10] Sunnersjö, C. S. Rolling bearing vibrations—The effects of geometrical imperfections and wear, *Journal of Sound and Vibration*, **98** (4), 455–474, (1985).

[11] Gupta, P. K. On the dynamics of a tapered roller bearing, *Journal of Tribology*, **111** (2), 278–287, (1989).

[12] Su, Y.-T., Lin, M.-H., and Lee, M.-S. The effects of surface irregularities on roller bearing vibrations, *Journal of Sound and Vibration*, **165** (3), 455–466, (1993).

[13] Ohta, H. and Sugimoto, N. Vibration characteristics of tapered roller bearings, *Journal of Sound and Vibration*, **190** (2), 137–147, (1996).

[14] Su, Y.-T. and Lin, S.-J. On initial fault detection of a tapered roller bearing: frequency domain analysis, *Journal of Sound and Vibration*, **155** (1), 75–84, (1992).

[15] Yang, Y., Danyluk, S., and Hoeprich, M. A study on rolling element skew measurement in a tapered roller bearing with a specialized capacitance probe, *Journal of Tribology*, **122** (3), 534–538, (2000).

[16] Tarawneh, C., Cole, K., Wilson, B., and Reed, M. A metallurgical and experimental investigation into sources of warm bearing trending, *Proceedings of the 2008 IEEE/ASME Joint Rail Conference*, Wilmington, Delaware, April 22–24, (2008).

[17] Tarawneh, C., Cole, K., Wilson, B., and Freisen, K. A lumped capacitance model for the transient heating of railroad tapered roller bearings, *Proceeding of the 2007 ASEE-GSW Annual conference*, March 28–30, (2007).

[18] Tarawneh, C., Cole, K., Wilson, B., and Alnaimat, F. Experiments and models for the thermal response of railroad tapered roller bearings, *International Journal of Heat and Mass Transfer*, **51**, 5794–5803, (2008).

[19] Tarawneh, C., Fuentes, A. A., Kypuros, J. A., Navarro, L. A., Vaipan, A. G., and Wilson, B. M. Thermal modeling of a railroad tapered roller bearing using finite element method, *Journal of Thermal Science and Engineering Applications*, **4** (3), 9–19, (2012).

[20] Tarawneh, C., Wilson, B. M., Cole, K. D., Fuentes, A. A., and Cardenas, J. M. Dynamic bearing testing aimed at identifying the root cause of warm bearing temperature trending, *Proceedings of the 2008 ASME RTD Fall Technical Conference*, RTDF2008–74036, Chicago, Illinois, September 24–26, (2008).

[21] Tarawneh, C., Kypuros, J. A., Wilson, B., Snyder, T. W., Fuentes, A. A., and Gonzalez, B. A. A collaborative on-track field test conducted to verify the laboratory findings of bearing temperature trending, *Proceedings of the 2009 ASME Joint Rail Conference*, Pueblo, Colorado, March 3–5, (2009).

[22] Tarawneh, C., Kypuros, J. A., Fuentes, A. A., Wilson, B. M., Gonzalez, B. A., Rodriguez, G., and Maldonado, R. K. Vibration signatures of temperature trended bearings in field and laboratory testing, *Proceedings of the 2009 ASME RTD Fall Technical Conference*, RTDF2009-18038, Ft. Worth, Texas, October 20–21, (2009).

[23] FFTW, Retrieved from http://www.fftw.org, (Accessed January 14, 2013).

[24] Frigo, M. and Johnson, S. G. FFTW: An Adaptive Software Architecture for the FFT, *Proceedings of the International Conference on Acoustics, Speech, and Signal Processing*, **3**, 1381–1384, (1998).

[25] Gonzalez, B. A. A study of the effect of vibration on railroad bearing temperature, M.S. Thesis, University of Texas Pan-American, Edinburg, Texas, (2010).